RSC Advances

PAPER

View Article Online
View Journal | View Issue

Cite this: *RSC Adv.*, 2021, **11**, 416

Polydimethylsiloxane nanocomposite macroporous films prepared *via* Pickering high internal phase emulsions as effective dielectrics for enhancing the performance of triboelectric nanogenerators†

José Miguel Blancas Flores,[a] María Guadalupe Pérez García,[a] Gabriel González Contreras,[b] Alberto Coronado Mendoza[a] and Victor Hugo Romero Arellano *[a]

Polydimethylsiloxane (PDMS) nanocomposite (NC) macroporous films were prepared by a Pickering high internal phase emulsion (HIPE) templating technique and used as effective dielectrics for enhancing the performance of triboelectric-nanogenerators (TENGs). HIPEs were formulated using commercial PDMS and water as the continuous and dispersed phase, respectively. The formation and solidification of PDMS-based HIPEs were possible through stabilization with silver-nanoparticles (Ag-Nps) and surfactant (Span 20) mixtures. The resulting PDMS-NC-polyHIPE films presented an interconnected 3D macroporous structure with Ag-Nps on their porous surface. The addition of different amounts of Ag-Nps (0, 4, 20, 28, 36 wt%) in HIPE formulations allowed modification of the pore size, total pore volume and dielectric properties of the tribo-materials. Results revealed that both the porosity and dielectric properties of these materials play an important role in enhancing the output performance of TENGs. Thus, the best TENG based on the PDMS-NC-polyHIPE film was achieved with 20 wt% of Ag-Nps, with voltage, current and power values of 4.88 V, 0.433 μA and 2.1 μW, respectively, which gives over 3.28-fold power enhancement compared with the reference TENG (based on a PDMS film without porosity or Ag-Nps). Therefore, the preparation of tribo-materials through a Pickering HIPE templating technique provides a novel, effective and easy way for the improvement of the TENG's performance.

Received 16th September 2020
Accepted 7th December 2020

DOI: 10.1039/d0ra07934k

rsc.li/rsc-advances

Introduction

Triboelectric nanogenerators (TENGs) have attracted a lot of attention due to their relatively high efficiencies, and large output power, as well as ease of manufacture, low materials costs, and great versatility of possible applications.[1–5] Since the emergence of TENGs, multiple proposals have been made for the improvement of these systems. On the one hand, optimization strategies have focused on device design and there is currently a wide variety of geometries and configurations,[5–11] while other proposals have focused on the modification of tribo-materials to enhance the energy conversion efficiency.[12–15]

Polydimethylsiloxane (PDMS) is commonly used as tribo-material due to its interesting properties such as electronegativity, flexibility, transparency and ease of large scale production.[12,14–16] Recently, special interest has been given to the fabrication of porous PDMS films (also known as sponges) because their porous structure provides better mechanical properties (*e.g.* flexibility and compressibility), which makes them attractive for the development of flexible electronic devices.[17–20] In order to improve the performance of these porous structures in TENG devices, it is common to create nanocomposite (NC) films by the incorporation of nanoparticles (Nps) such as Ag, Au, TiO_2, SiO_2, or $BaTiO_3$ as fillers in PDMS arrays, with which micro-capacitor structures are created, obtaining improvements in electrical properties, thus achieving a more efficient output-power.[21–23] Currently, there are several methods and strategies for the development of PDMS NC sponges,[24] however only some of them have been evaluated in TENGs. For instance, the direct template method has been widely used due to its simplicity as it does not require additional equipment for its preparation.[15,19–23,25–29]

The typical procedure of the direct template method consists to prepare a mixture between the elastomer, the filler dielectric

[a]*Centro Universitario de Tonalá, División de Ingenierías e Innovación Tecnológica, Universidad de Guadalajara, Tonalá, Jal. 45425, Mexico. E-mail: vicromare@gmail.com*

[b]*Cátedras CONACYT, Coordinación para la Innovación y la Aplicación de la Ciencia y la Tecnología, Universidad Autónoma de San Luis Potosí, San Luis Potosí, 78000, Mexico*

† Electronic supplementary information (ESI) available. See DOI: 10.1039/d0ra07934k

nanoparticles and some kind of particle that will be later dissolved to generate the porous structure, Xia, *et al.*[23] used sugar particles of different sizes and at different concentrations and silver nanoparticles (Ag-Nps) as fillers. After the elimination of sugar particles, porous structures with embedded Ag-Nps were obtained and used as tribo-materials of TENGs. These devices achieved an output power as high as 6 W m^{-2} due to an increase in current output 4 times greater than TENGs based on solid PDMS films. In other work, Chen *et al.*[21] used NaCl particles to create the porous structure and made a comparison between different filler dielectric Nps (SiO_2, TiO_2, $BaTiO_3$ and $SrTiO_3$). The obtained tribo-materials reached an output power of 6.47 W m^{-2} equivalent to 5 times the power improvement compared to the reference TENG. In both reports, the pore size was limited to the size of the dissolved particles, and the interconnection of the pores is not favored due to the relative separation between the incorporated particles. In addition, long washing processes were required to dissolve the particles to obtain the porous structure.

On the other hand, Chun *et al.*[22] added water during the PDMS curing process, which was later evaporated to obtain materials with different porous structures depending on the amount of water incorporated to the PDMS elastomer. Then, the porous structure was impregnated with gold nanoparticles (Au-Nps). The resulting NC porous tribo-materials achieved an output-power of 13 mW, 5-fold power enhancement compared with a flat film-based TENG, which was, attributed to the density of charges created by the contact between Au-Nps and PDMS inside the pores. However, the impregnation process involves long times, and requires good pore interconnection, to ensure a uniform distribution of Au-Nps.

In all the previous reports mentioned, the effects achieved are directly related to the concentration and nature of the incorporated Nps, as well as the interconnection, size and volume of pores. Thus, the implementation of alternative techniques that allows a better control of porous structure and surface functionalization with Nps in the development of NC porous tribo-materials is of great interest nowadays.

In this context, emulsion templating is a versatile technique widely employed to prepare highly porous and well-defined porous materials, whereby the droplets of the internal (or dispersed) phase are used to create the porous structure by curing or polymerization of the continuous phase.[30] Regarding high internal phase emulsions (HIPEs), the internal volume fraction accounts for more than 74%, which allows the formation of polyhedral drops in the range of micrometers that, upon solidification of the continuous phase and extraction of the internal one, result in interconnected 3D macroporous materials commonly known as polyHIPEs.[30–32] The porous structure and thus the specific surface area of these materials is tailored by altering the type or concentration of surfactant, the internal to continuous phase volume ratio, and the cross-linked concentrations used in HIPEs formulation.[33–36] In addition, the incorporation of particles can replace or reduce the amount of surfactant increasing the emulsion stability due to particles tendency to adsorb quasi-irreversibly to the oil–water interface, which avoid coalescence and Ostwald ripening.[37–39] These emulsions are termed Pickering HIPEs. It has been reported that nanoparticles and surfactants synergistically used to stabilize the emulsion not only allow to control pore size, pore openness and interconnectivity, but also provide a suitable method of surface porous functionalization of the resulting nanocomposite (NC) polyHIPEs.[40–42]

NC-polyHIPEs have found several applications where the control of the porous structure and the surface functionalization with nanoparticles is crucial, many of which involves support for chemical reactions,[43] absorbents for water purification,[41,44] tissue engineering,[45–47] among others. Such control of the porous structure and the surface functionalization with nanoparticles have become also crucial to the development of tribo-materials for enhancing the TENGs performance.[48] Draws attention that although the Pickering HIPE templating technique could provide several advantages in this matter, until now, there is no report of NC-polyHIPEs applied as tribo-materials.

In addition, there are few works reported about PDMS-based polyHIPEs, which could be attributed to viscosity-related processing challenges associated with commercially-available PDMS used as the continuous phase in HIPEs formulation. For instance, Kataruka *et al.*,[49] produced Pickering HIPE templates (stabilized by silica nanoparticles and the Gransurf 2106 surfactant) *via* centrifugation of low internal phase emulsions (LIPEs, <30% by volume dispersed phase) to overcome the prohibitive barrier to HIPE formation when using a mechanically-superior, but highly viscous commercial PDMS kit. Open and closed-cell NC-polyHIPEs were obtained where the porous structure and interconnectivity depended on the centrifugation force and the emulsifier. In a different approach, Kovalenko *et al.*,[50] showed that using surfactants with different solubility in the high viscous continuous phase (PDMS) and mixing them by a mechanical stirring, it was possible to tune the emulsions droplets, which leaded to modify the porous structure of the resulting materials. Furthermore, it was observed that the mechanical and acoustic properties of the porous materials were improved by tailoring the porous structure.

In this work, PDMS-NC-porous films were synthesized through the Pickering HIPE templating technique and used as tribo-materials of vertical-contact-mode TENG system. The pore size, total pore volume and dielectric properties of these materials were easily modified by the addition of different amounts of Ag-Nps (0, 4, 20, 28 and 36 wt%) and the surfactant Span 20 (0 and 1 wt%) in HIPEs formulation. For comparative purposes, flat PDMS-NC films with different amounts of Ag-Nps (0 and 20 wt%) were also used as tribo-materials of TENGs. The effect of the pore size, total pore volume and the amount of Ag-Nps on the output response of TENG was systematically studied. Finally, the Pickering HIPE templating technique is presented as a novel strategy to control the porous structure as well as the porous surface functionalization with Ag-Nps as effective dielectrics of triboelectric PDMS-NC porous materials for enhancing TENGs' performance.

Experimental

Materials

Polydimethylsiloxane (PDMS) Sylgard® 184 silicon (elastomer and curing agent). Distilled water, surfactant Span® 20, sodium chloride (NaCl, 99.0%), silver nitrate ($AgNO_3$, 99.0%), sodium citrate ($Na_3C_6H_5O_7$, 99.0%), sodium borohydride ($NaBH_4$, 98.0%), and poly(*N*-vinylpyrrolidone) (PVP-40). All reagents were obtained from Sigma-Aldrich. For the assembly of the TENG devices, 2 × 2 cm copper foils were used as conductive electrodes.

Synthesis and characterization of silver nanoparticles

Silver nanoparticles (Ag-Nps) with 11.8 nm average diameter were prepared by the reduction method according to a modified synthesis procedure.[51] In a typical synthesis, $AgNO_3$ (2 mg) and sodium citrate (2 mg) were mixed in distilled water (35 mL). Afterwards, the mixture is cooled by placing it in a container with ice, under constant stirring, then $NaBH_4$ (1 mL, 10 mmol) was added to the reaction mixture, and finally, PVP (1 mL, 25 mmol) was added and stirred for 3 h. The final solution was washed with distilled water in a centrifuge at 15 000 rpm for 15 min, and the obtained precipitate was redispersed in 10 mL of distilled water.

The morphology of Ag-Nps was observed by transmission electron microscopy (TEM, JEM ARM 200 CF). The average size and size distribution were obtained by dynamic light scattering (DLS, Malvern Zetasizer Nano ZS90).

Preparation of PDMS films

PDMS-nanocomposite (NC)-porous films were synthesized through the Pickering high-internal-phase emulsions (HIPEs) templating technique. For this purpose, water-in-PDMS HIPEs were obtained by dropwise addition with stirring of the dispersed phase (aqueous solution containing 1.5 wt% NaCl) accounting for 80 vol% (4 mL) to the continuous phase accounting for 20 vol% (1 mL) in a 10 mL glass vial at 25 °C. The continuous phase was prepared by mixing Sylgard 184 silicone elastomer (1 g) with different amounts of the surfactant Span 20 (0 and 1 wt% with respect to the total weight of the emulsion) and colloidal Ag-Nps (0, 4, 20, 28 and 36 wt% with respect to the total weight of the emulsion). Mechanical stirring was applied with a home-made helical device until a white homogeneous emulsion was obtained. To obtain the PDMS-NC-porous films, Sylgard 184 silicone curing agent (0.1 g) was added to the emulsions and stirred for 20 min. Then, the HIPEs were deposited between two glass plates with an area of 4.00 ± 0.07 cm^2, and cured at 65 °C for 24 h. After HIPEs curing, the internal phase and the surfactant were removed by washing with water for 48 h and then with ethanol for 24 h. Finally, the polyHIPEs films were dried at 65 °C until constant weight was reached, and were labelled as polyHIPE@*X* where *X* was the amount of the colloidal Ag-Nps. In addition, flat PDMS-NC films (without porosity) were prepared by mixing Sylgard 184 silicone elastomer base (1 g) and curing agent (0.1 g) in a 10 : 1 mass ratio, respectively, with different amount of colloidal Ag-Nps (0, 4, 20, 28 and 36 wt% with respect to the total weight of the emulsion) and labelled as F-PDMS@*X* were *X* was the amount of the colloidal Ag-Nps. The mixtures were deposited between two glass plates with an area of 4.00 ± 0.07 cm^2, and cured at 65 °C for 24 h.

Characterization of HIPEs and nanocomposite porous films

HIPEs were observed by optical microscopy (Olympus BX51) with a camera QICAM (FAST1394) and the software Linksys 32. The droplet size was determined using ImageJ analysis software as the average of 100 image readings. The macroporous structure of the polyHIPEs films was observed by field emission scanning electron microscopy (FESEM; Mira from TESCAN) at an accelerating voltage of 10 kV. All samples were gold-coated. The diameters of the pores were calculated by ImageJ analysis software as the average of 100 image readings.

The total pore volume (V_T) was estimated as $1/\rho_b - 1/\rho_w$ where ρ_b is the polyHIPE film density and ρ_w is the wall density of pores that is the density of the NC polymer (curing PDMS/Ag-Nps nanocomposite). ρ_w corresponded to the density of the flat PDMS film containing the same amount of Ag-Nps than the respective polyHIPE film. ρ_b and ρ_w were calculated by measuring the volume and weight of the polyHIPE and flat PDMS films, respectively.

X-ray diffraction (XRD) patterns of polyHIPE films were collected by using an Empyrean diffractometer (Cu Kα radiation, 0.02° step size and 30 s counting time). In addition, polyHIPEs films were analysed by energy dispersive X-ray spectroscopy (EDS) using a Bruker AXS. To verify the presence of Ag-Nps onto the porous surface of the films, EDS analysis was performed at different points of the samples.

Design and testing of triboelectric nanogenerator

The different PDMS-nanocomposite films were assembled as vertical contact-separation mode TENG. They were placed on copper foil (2 × 2 cm) at the bottom of vibration exciter and cover with other copper foil on the top, and conducting wires were connected to the two copper electrodes for subsequent electric measurement. A repeated press and release process with cyclic vertical movements of 5.5 mm maximum displacement was performed using a home-made vibration exciter (3 N force, and 25 Hz frequency). Capacitance of the PDMS-nanocomposite films was measured by LCR meter (UNI-T UT612), and electrical characterization was performed by an oscilloscope (UNI-T UTD4204C). The voltage and current values were obtained by taking the average of the peak-voltage and peak-current measurements respectively.

Results and discussion

Stabilization and morphology of water-in-PDMS Pickering HIPEs

The control of the porous structure and the porous surface functionalization with metallic nanoparticles represent a great challenge nowadays in the development of tribo-materials for enhancing the TENGs performance. In this regard, although

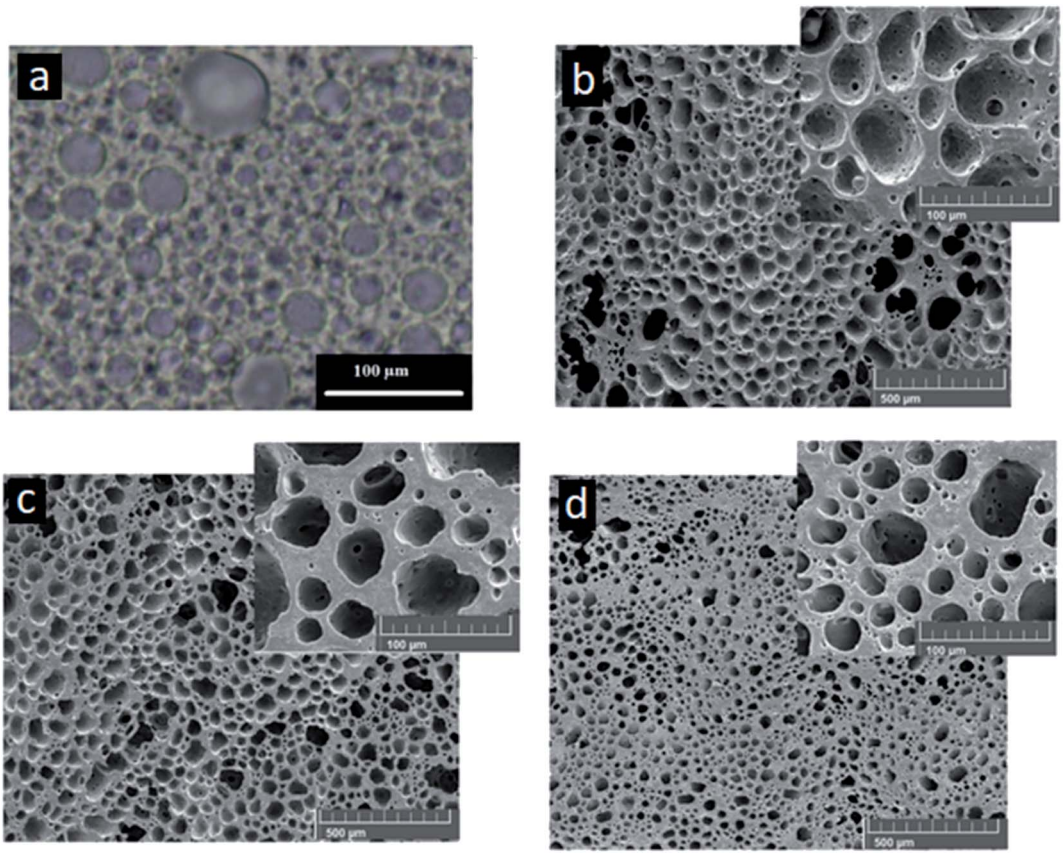

Fig. 1 (a) Optical micrograph of HIPE with 36 wt% of Ag-Np and (b, c and d) FESEM micrographs at different magnifications of polyHIPEs films after washing and drying: (b) polyHIPE@20, (c) polyHIPE@28 and (d) polyHIPE@36.

NC-polyHIPEs have been considered for numerous applications where the control of the porous structure and porous surface functionalization with nanoparticles are required,[41,43–47] until now there is no report of NC-polyHIPEs applied as tribomaterials. Herein, the Pickering HIPE templating technique is explored as a novel strategy in the development of tribomaterials. For this purpose, water-in-PDMS Pickering HIPEs were formulated with different amount of colloidal Ag-Nps (0, 4, 20, 28 and 36 wt%) and surfactant Span 20 (0 and 1 wt%). Emulsions prepared without surfactant and with the different amount of Ag-Nps were not stable and presented phase separation. It has been reported that nanoparticles can be used as a single effective emulsifier for droplet size-controlled emulsion production when their adsorption kinetics supports the formation of an effective barrier at the interface.[42,52,53] If the effective adsorption barrier is not formed only with nanoparticles, molecular surfactants can increase stabilization of the emulsion by-co-stabilization.[41,42,52,53] Thus, HIPEs stability was achieved with a low amount of the surfactant Span 20 (1 wt%). These emulsions had a white aspect (Fig. S1a†), presented high viscosity (they did not flow upon inversion of the containers) and were stable for more than 24 h. Span 20 was a suitable surfactant in the formulation of stable HIPEs mainly due to its low hydrophilic/lipophilic balance value (HLB) of 8.6 and its easy dissolution in PDMS. It has been reported[54] that the phase in which the surfactant is the most soluble tends to be the continuous phase of the emulsion. In this case, PDMS is a hydrophobic continuous phase and thus, the production of stable water-in-PDMS HIPEs required a surfactant with a low HLB value. The surfactant Span 20 was soluble in PDMS and not in the aqueous phase, which could explain the formation of stable emulsions.

The morphology of HIPEs consisted of close-packed polyhedral and polydisperse droplets separated by a thin film of the continuous phase (PDMS), as was observed by optical microscopy (Fig. 1a shows a representative optical micrograph of HIPE with 36 wt% of Ag-Nps). In addition, the droplet size decreased as the amount of Ag-Nps increased and the amount of the surfactant Span 20 remained constant (Fig. 2). An increase in droplet size has been attributed to coalescence between droplets, which could be an indicative of low emulsion stability.[41,42] The results suggest that Ag-Nps form an effective adsorption barrier at the W/O interface that prevents coalescence. Thus, a more compact droplet conformation can be observed when the amount of Ag-Nps increased. Furthermore, the effective barrier at the interface is not formed only with Ag-Nps, but a low amount of the surfactant Span 20 (1 wt%) was required to obtain the stable emulsions. The dual emulsifiers synergism between the surfactant and nanoparticles leads to an enhanced emulsion stability, as was reported in previous works.[42,52–54]

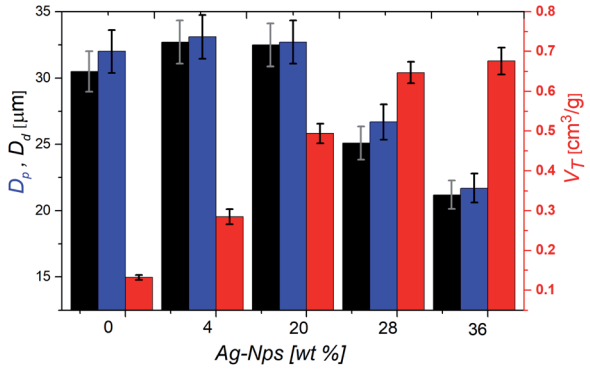

Fig. 2 Droplet diameter (D_d, black bars), pore diameter (D_p, blue bars) and total pore volume (V_T, red bars) of polyHIPEs films as a function of Ag-Nps amount.

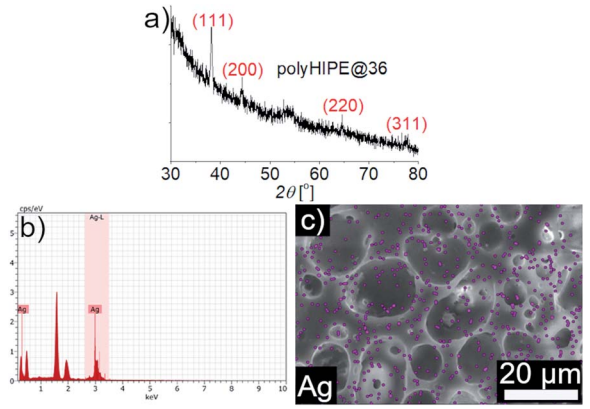

Fig. 3 (a) XRD pattern, (b) spectra EDS and (c) elemental mapping of polyHIPE@36 film.

Ag-Nps used in HIPEs formulation were prepared by a reduction method[51] and chosen for this study mainly because their dielectric properties (advantageous for the development of the tribo-material).[23,55] Fig. S2,† shows a TEM micrograph and the inset shows the size distribution obtained by DLS analysis of the synthesized Ag-Nps. Results revealed that Ag-Nps were quasi spherical (Fig. S2†) and with an average size of 11.8 ± 0.70 nm.

Porous structure, surface and total pore volume of nanocomposite polyHIPEs films

Upon curing of the PDMS phase and extraction of the aqueous phase, HIPEs resulted in PDMS-NC porous films (Fig. S1b†). The porous morphology of these materials was observed by field emission electron microscopy (FESEM). FESEM micrographs (Fig. 1b–d and S3†) show that the macroporous structure of the polyHIPEs films consisted of a non-spherical cell network with cells interconnected through pore windows. The non-spherical cells resembled the polyhedral droplets characteristic of HIPEs (Fig. 1). The pore sizes (D_p) of all polyHIPEs were similar to the droplet sizes (D_d) of their respective HIPEs used as templates (Fig. 2). These results indicate that the precursor HIPEs presented high stability during the curing process. As it was expected, D_p decreased as the amount of Ag-Nps used in HIPEs formulation increased.

According with previous works,[43,56] the total pore volume (V_T) can be estimated as $1/\rho_b - 1/\rho_w$ where ρ_b is the polyHIPE film density and ρ_w is the wall density of pores that is the density of the NC polymer (curing PDMS/Ag-Nps nanocomposite). In this case, ρ_w values can be corresponded to the density of flat PDMS films containing the same amount of Ag-Nps than polyHIPE films. Therefore, ρ_w and ρ_b were estimated by measuring the volume and weight of the polyHIPE and flat PDMS films with the different amounts of Ag-Nps, as was explained in the experimental section. Flat PDMS films with 0, 4, 20, 28 and 36 wt% of Ag-Nps presented ρ_w values of 0.96, 1.14, 1.44, 1.46, and 1.47 g cm^{-3}, respectively. In the case of porous PDMS films, polyHIPE@0, polyHIPE@4, polyHIPE@20, polyHIPE@28 and polyHIPE@36 presented ρ_b values of 0.85, 0.86, 0.84, 0.75 and 0.73 g cm^{-3}, respectively. ρ_b and ρ_w were used to estimate V_T values of all polyHIPEs. Fig. 2 shows that V_T increased as D_p decreased; this behaviour is similar to those reported in previous works.[36,56] It is evident that D_p and V_T can be modified by the addition of different amounts of Ag-Nps in HIPEs formulation.

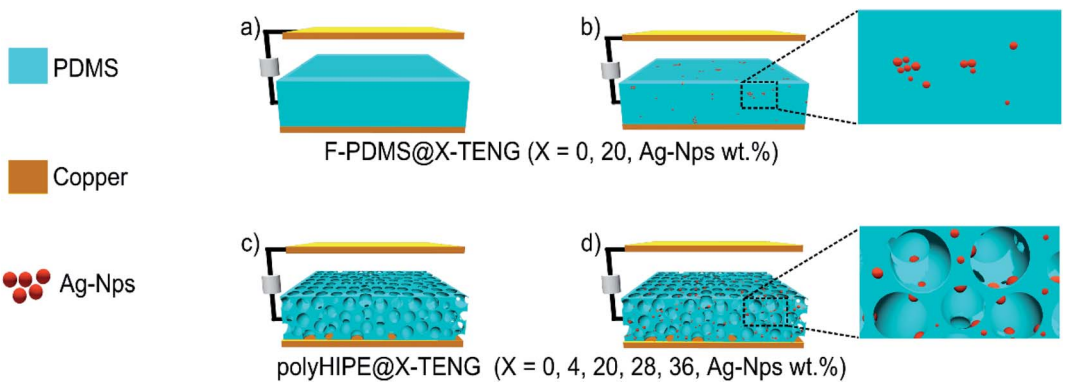

Fig. 4 Schematic representation of vertical contact-separation mode TENGs with the different PDMS-nanocomposite films configurations. (a and b) TENG with flat PDMS film without pores, (a) F-PDMS@0-TENG and (b) F-PDMS@36-TENG. (c and d) TENGs with porous PDMS films (c) polyHIPE@0-TENG, (d) polyHIPE@X-TENG, (X = 4, 20, 28, 36 Ag-Nps wt%).

Table 1 Thickness (d), capacitance (C), relative dielectric constant (ε_r) and dielectric loss (tan δ) of polyHIPE@X films and flat PDMS films (F-PDMS@X)

Sample	d [mm]	C [pF]	ε_r	tan δ $\times 10^{-3}$
PolyHIPE@0	0.47	22.60 ± 0.40	3.00 ± 0.02	3.19
PolyHIPE@4	0.47	24.15 ± 0.10	3.21 ± 0.10	3.19
PolyHIPE@20	0.46	24.64 ± 0.20	3.20 ± 0.01	3.26
PolyHIPE@28	0.46	23.45 ± 1.05	3.05 ± 0.04	3.26
PolyHIPE@36	0.45	23.90 ± 0.50	3.04 ± 0.01	3.34
F-PDMS@0	0.47	22.90 ± 0.40	3.04 ± 0.01	3.19
F-PDMS@20	0.47	21.40 ± 0.50	2.84 ± 0.02	3.19

X-ray diffraction (XRD) analysis confirmed the presence of Ag-Nps in polyHIPEs films (Fig. 3a shows the XRD pattern of polyHIPE@36). The diffraction peaks were located at 38.11°, 44.33°, 64.60° and 77.47° that can be indexed to (111), (200), (220) and (311) planes, respectively, corresponding to the face centered cubic phase of silver (JCPDS file no. 04-0783). Furthermore, EDS spectra and elemental mapping exposed the presence of the Ag-Nps onto the porous surface of the polyHIPE films, (Fig. 3b and c are shown as representative results).

Electrical measurements

To facilitate the discussion, the studied TENG systems with the different PDMS films are represented in Fig. 4, which have been labelled according to the film used, polyHIPE@X-TENG for porous PDMS films and F-PDMS@X-TENG for flat PDMS films. The thickness and electrical measurements of each NC-films are summarized in Table 1. The expression of capacitance (C) of an ideal parallel plate capacitor[23] was used to analyse the electrical properties of the PDMS films (eqn (1)).

$$C = \frac{\varepsilon_0 \varepsilon_r S}{d} \quad (1)$$

where ε_0 is the permittivity of the vacuum, ε_r is the relative permittivity, S is the surface area of the electrode and d is the thickness of the PDMS films. The capacitance measured at 100 kHz, dielectric loss, relative permittivity and thickness of the different porous and not porous films in function of Ag-Nps wt% can be analysed in Table 1.

Initially, both the capacitance and relative permittivity of the polyHIPE@4 film show an increase with respect to the reference film (polyHIPE@0), then, when increasing the amount of silver (polyHIPE@20), the capacitance increases slightly, while the relative permittivity remains almost constant; later, when the Ag-Nps exceeds 20 wt%, both the relative permittivity and capacitance begin to decrease.

The same tendency discussed above was obtained in the curves of the open-circuit voltage and short-circuit current *versus* time for the different assembled TENGs, which are shown in Fig. 5a and b, respectively. The initial generated output short-circuit current and open-circuit voltage for the polyHIPE@0-TENG were 0.261 μA and 2.61 V, respectively, later these values increased with the rise of Ag-Nps, reaching a maximum of 0.433 μA and 4.88 V for current and voltage for the polyHIPE@20-TENG which represents a 66% and 87% increment, respectively, with respect to the reference polyHIPE@0-TENG. Finally, the output short-circuit current and open-circuit voltage of the TENGs decreased when Ag-Nps were greater than 20%.

The non-linear variation of the electrical properties has been reported by other authors as a consequence of different factors. For the systems studied in this work, the total pore volume (see Fig. 2) and dielectric loss increases with the concentration of Ag-Nps. Both parameters contribute to reduce the electrical properties, the effect of deterioration due to the presence of pores can be explained in terms of the effective permittivity, that consists of a combination of the relative permittivity values of the PDMS film and the permittivity of air $\varepsilon_r = 1$ present inside of the pores gap,[21] while the dielectric loss represents a reduction of the charge storage.[23] Likewise, another parameter that represents deterioration of the electrical properties is the saturation of Ag-Nps, which increases the leakage current, thus reducing the effect of triboelectrification as reported by Park *et al.*[57]

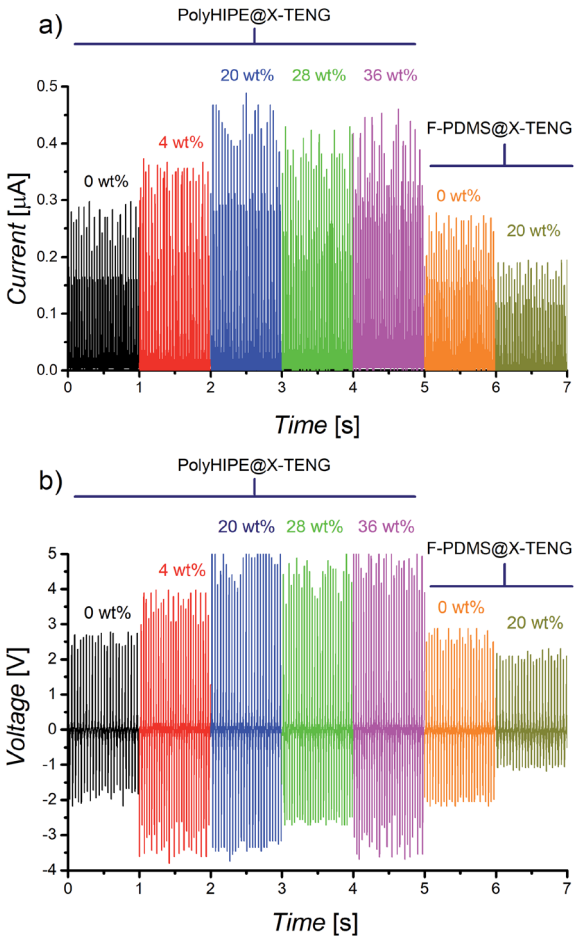

Fig. 5 (a) Output short-circuit current (μA), (rectified signal using a diode bridge and a parallel connected resistance of 2.7 MΩ) and (b) open-circuit voltage (V_{oc}) *versus* time, generated by the different TENGs systems.

On the other hands, there are parameters that favor the electrical properties, one of them is the reduction of the thickness of the dielectric film, that was reduced with the amount of Ag-Nps, starting with an initial thickness of 0.47 mm for the sample without Ag-Nps (polyHIPE@0), and decreasing up to 0.45 mm for the maximum amount of Ag-Nps (polyHIPE@36). Similarly, a factor for the improvement of the electrical properties is the formation of capacitor structures due to the interaction between a metal and a dielectric (Ag-Nps and PDMS respectively), defined by Xia *et al.*,[23] as variable micro capacitors (VMCs) in arrays of cellular structures formed in a porous network, in this way, when compression is applied to the film, the diameter of the pores will decrease, thus improving the capacitance.

As discussed above, porous structures can represent a deterioration in electrical properties due to the presence of air in the pore gap, however at the same time, a film with a porous structure presents a greater contact area, as well as better compressibility,[21,22] in this way, the best balance between all of this effects was achieved for sample polyHIPE@20, and the decrease in electrical properties for samples polyHIPE@28 and polyHIPE@36, suggests that the effect of the formation of silver aggregates begins to predominate. It should be noted that for the same amount of Ag-Nps embedded in a porous film (polyHIPE@20) and a non-porous film (F-PDMS@20), a higher density of nanoparticles will be generated in the porous films,[58] however it can be analyzed from Table 1, that the capacitance and dielectric constant values were lower for F-PDMS@20, (21.4 pF and $\varepsilon_r = 2.84$ respectively), this shows that the formation of nanoparticles aggregates becomes more sensitive in non-porous films, while at the same concentration, the dispersion of the nanoparticles in porous structures favors the effect of VMCs.

In order to analyze the effect of the porous structure without the influence of Ag-Nps, polyHIPE@0 and F-PDMS@0 films were compared. As expected, the dielectric constant and capacitance values were higher for the F-PDMS@0 film ($\varepsilon_r =$ 3.04 and 22.9 pF respectively), while dielectric loss and thickness of the films remained constant. As already discussed, the porous film shows lower electrical properties, as a consequence of a decreased in the effective permittivity due to the air present inside the pores gap.[21] However, it should be considered that these electrical properties were characterized with the films at rest, while the characterization of the performance of the TENGs devices is carried out under cyclical contact conditions (compression and relaxation). Under these considerations, in Table 2 it shows that the best performance between these two samples was obtained for polyHIPE@0-TENG, with an output current of 0.261 μA, and an output power of 0.68 μW. Therefore, the importance of a porous structured film is highlighted, because it has a greater contact area and reduces its thickness much better when subjected to compression,[21,22] both of these parameters are crucial for the $\varepsilon_r S/d$ ratio from eqn (1). However, we are aware that a broader study must take place in order to understand the contribution of every single parameter of the system.

Table 2 Electrical performance of polyHIPE@*X*-TENG and F-PDMS@*X*-TENG

Sample	Voltage [V]	Current [μA]	Power [μW]
PolyHIPE@0-TENG	2.61	0.261	0.68
PolyHIPE@4-TENG	3.53	0.359	1.27
PolyHIPE@20-TENG	4.88	0.433	2.10
PolyHIPE@28-TENG	4.34	0.377	1.64
PolyHIPE@36-TENG	4.67	0.388	1.81
F-PDMS@0-TENG	2.65	0.241	0.64
F-PDMS@20-TENG	2.01	0.173	0.35

Thus, the best triboelectric properties were obtained for the polyHIPE@20-TENG configuration with an output power of 2.1 μW which is 6 and 3.28 times greater than the F-PDMS@20-TENG and F-PDMS@0-TENG respectively, which makes it viable for low consumption devices, such as power LEDs. A proof of concept is presented in the ESI (Fig. S4†). These gain obtained represents values equivalent to the percentages of improvement reported in similar works,[21–23] which is an indication that the HIPEs technique is a competitive method with the possibility of creating capacitor structures with interconnected pores.

Conclusions

In this work, the Pickering HIPE templating technique is proposed for the first time as a simple and practical method to obtain porous PDMS films as dielectric materials to assemble in vertical contact-separation mode TENGs. Commercial PDMS and distilled water were used as continuous and dispersed phases, respectively. Mixture of surfactant (Span 20) and Ag-Nps were used as stabilizer agents of the emulsions. Ag-Nps were not only used to increase emulsion stability, but also to surface functionalization which allowed the formation of capacitor structures. The pore size, total pore volume and dielectric properties of the tribo-materials were easily modified by the addition of different amount of Ag-Nps. The results showed that the performance of TENGs systems are dependent on multiple factors, obtaining the best balance for the polyHIPE@20-TENG, with output open-circuit voltage, short-circuit current and power of 4.88 V, 0.433 μA and 2.1 μW, respectively. These value were equivalent to an increase in out-power of 6 and 3.28 times greater than the F-PDMS@20-TENG and F-PDMS@0-TENG respectively, respectively. This study opens the path to use of the HIPE templating technique as a suitable method to obtain nanocomposite porous tribo-materials applied to enhance TENGs performance. Certainly, there is plenty of room for further studies aiming to improve the dielectric properties of tribo-materials (and thus the output response of TENGs) by means of change the type of polymer used as continuous phase, the size and nature of nanoparticles, type and concentration of surfactant, the internal to continuous phase volume ratio, *etc.*, in HIPEs formulation. Thus, we hope that this work serves as departing point.

Conflicts of interest

There are no conflicts to declare.

Acknowledgements

Financial support for this work was provided by the "Fondo de Desarrollo Científico de Jalisco" (FODECIJAL, 8098-2019). G. G. would like to acknowledge support by the program Cátedras Conacyt through project 1757 and from project A1-S-43579 of SEP-CONACYT Ciencia Básica. The authors thank MC. Nicolás Haro and Dr Arturo Contreras for technical support in electrical measurement equipment, both professors of the CUTonalá of the University of Guadalajara.

References

1 L. Zhou, D. Liu, J. Wang and Z. L. Wang, *Friction*, 2020, **8**, 481.
2 J. Wang, Y. Zi, S. Li and X. Chen, *MRS Energy Sustain.*, 2020, **7**, 1.
3 W. Tang, T. Jiang, F. R. Fan, A. F. Yu, C. Zhang, X. Cao and Z. L. Wang, *Adv. Funct. Mater.*, 2015, **25**, 3718.
4 X. Cheng, L. Miao, Y. Song, Z. Su, H. Chen, X. Chen, J. Zhang and H. Zhang, *Nano Energy*, 2017, **38**, 438.
5 G. Zhu, P. Bai, J. Chen, Q. Jing and Z. L. Wang, *Nano Energy*, 2014, **14**, 126.
6 Y. Zi, H. Guo, J. Wang, Z. Wen, S. Li, C. Hu and Z. L. Wang, *Nano Energy*, 2017, **31**, 302.
7 S. Wang, L. Lin, Y. Xie, Q. Jing, S. Niu and Z. L. Wang, *Nano Lett.*, 2013, **13**, 2226.
8 L. Zhang, B. Zhang, J. Chen, L. Jin, W. Deng, J. Tang, H. Zhang, H. Pan, M. Zhu, W. Yang and Z. L. Wang, *Adv. Mater.*, 2016, **28**, 1650.
9 G. Zhu, P. Bai, J. Chen and Z. L. Wang, *Nano Energy*, 2013, **2**, 688.
10 W. Tang, C. Zhang, C. B. Han and Z. L. Wang, *Adv. Funct. Mater.*, 2014, **24**, 6684.
11 S. L. Zhang, M. Xu, C. Zhang, Y. C. Wang, H. Zou, X. He, Z. Wang and Z. L. Wang, *Nano Energy*, 2108, **48**, 421.
12 G. Suo, Y. Yu, Z. Zhang, S. Wang, P. Zhao, J. Li and X. Wang, *ACS Appl. Mater. Interfaces*, 2016, **8**, 34335.
13 Y. Yu and X. Wang, *Extreme Mech. Lett.*, 2016, **9**, 514.
14 B. K. Yun, J. W. Kim, H. S. Kim, K. W. Jung, Y. Yi, M. S. Jeong, J. H. Ko and J. H. Jung, *Nano Energy*, 2015, **15**, 523.
15 F. R. Fan, L. Lin, G. Zhu, W. Wu, R. Zhang and Z. L. Wang, *Nano Lett.*, 2012, **12**, 3109.
16 X. Xinze, L. Chao, W. Gong, X. Ying, W. Jiping and Y. Hai, *Chem. Res. Chin. Univ.*, 2015, **31**, 434.
17 B. Y. Lee, J. Kim, H. Kim, C. Kim and S. D. Lee, *Sens. Actuators, A*, 2016, **240**, 103.
18 X. He, X. Mu, Q. Wen, Z. Wen, J. Yang, C. Hu and H. Shi, *J. Appl. Mech.*, 2018, **85**, 041009.
19 X. He, X. Mu, Q. Wen, Z. Wen, J. Yang, C. Hu and H. Shi, *Nano Res.*, 2016, **9**, 3714.
20 K. Y. Lee, J. Chun, J. H. Lee, K. N. Kim, N. R. Kang, J. Y. Kim, M. H. Kim, K. S. Shin, M. K. Gupta, J. M. Baik and S. W. Kim, *Adv. Mater.*, 2014, **26**, 5037.
21 J. Chen, H. Guo, X. He, G. Liu, Y. Xi, H. Shi and C. Hu, *ACS Appl. Mater. Interfaces*, 2016, **8**, 736.
22 J. Chun, J. W. Kim, W. S. Jung, C. Y. Kang, S. W. Kim, Z. L. Wang and J. M. Baik, *Energy Environ. Sci.*, 2015, **8**, 3006.
23 X. Xia, J. Chen, H. Guo, G. Liu, D. Wei, X. Wang and C. Hu, *Nano Res.*, 2017, **10**, 320.
24 D. Zhu, S. H. Wang and X. Zhou, *J. Mater. Chem. A*, 2017, **5**, 16467.
25 D. Tantraviwat, P. Buarin, S. Suntalelat, W. Sripumkhai, P. Pattamang, G. Rujijanagul and B. Inceesungvorn, *Nano Energy*, 2020, **67**, 104214.
26 Y. Tang, Q. Zheng, B. Chen, Z. Ma and S. Gong, *Nano Energy*, 2017, **38**, 401.
27 X. Li, C. Jiang, F. Zhao, L. Lan, Y. Yao, Y. Yu, J. Ping and Y. Ying, *Nano Energy*, 2019, **61**, 78.
28 L. Zhang, L. Jin, B. Zhang, W. Deng, H. Pan, J. Tang, M. Zhu and W. Yang, *Nano Energy*, 2015, **16**, 516.
29 C. Jiang, X. Li, Y. Yao, L. Lan, Y. Shao, F. Zhao, Y. Ying and J. Ping, *Nano Energy*, 2019, **66**, 104121.
30 T. Zhang, R. A. Sanguramath, S. Israel and M. S. Silverstein, *Macromolecules*, 2019, **52**, 5445.
31 S. Sadeghi and M. R. Moghbeli, *Colloids Surf., A*, 2012, **409**, 42.
32 M. S. Silverstein, *Prog. Polym. Sci.*, 2014, **39**, 199.
33 K. J. Lissant, *J. Colloid Interface Sci.*, 1966, **22**, 462.
34 L. L. C. Wong, P. M. Baiz V, A. Menner and A. Bismarck, *Langmuir*, 2013, **29**, 5952.
35 N. Teo and S. C. Jana, *Langmuir*, 2017, **33**, 12729.
36 A. Davis, S. Surdo, G. Caputo, I. S. Bayer and A. Athanassiou, *ACS Appl. Mater. Interfaces*, 2018, **10**, 2907.
37 M. G. Pérez-García, A. Carranza, J. E. Puig, J. A. Pojman, F. del Monte, G. Luna-Bárcenas and J. D. Monta-Morales, *RSC Adv.*, 2015, **5**, 23255.
38 I. Zafeiri, C. Horridge, E. Tripodi and F. Spyropoulos, *Colloid Interface Sci. Commun.*, 2017, **17**, 5.
39 Y. Chevalier and M. A. Bolzinger, *Colloids Surf., A*, 2013, **439**, 23.
40 S. U. Pickering, M. A. and F. R. S., *J. Chem. Soc., Trans.*, 1907, **91**, 2001.
41 D. Yin, Y. Guan, B. Li and B. Zhang, *Colloids Surf., A*, 2016, **506**, 550.
42 A. Carranza, M. G. Pérez-García, K. Song, G. M. Jeha, Z. Diao, R. Jin, N. Bogdanchikova, A. F. Soltero, M. Terrones, Q. Wu, J. A. Pojman and J. D. Mota-Morales, *ACS Appl. Mater. Interfaces*, 2016, **8**, 31295.
43 S. A. García-Landeros, J. M. Cervantez-Díaz, A. Gutiérrez-Becerra, J. B. Pelayo-Vázquez, G. Landazuri-Gomez, J. Herrera-Ordonez, J. F. A. Soltero-Martínez, J. D. Mota-Morales and M. G. Pérez-García, *Chem. Commun.*, 2019, **55**, 12292.
44 S. Zhang, X. Fan, F. Zhang, Y. Zhu and J. Chen, *Langmuir*, 2018, **34**, 3669.
45 Y. Zhu, W. Wang, H. Yu and A. Wang, *J. Environ. Sci.*, 2020, **88**, 217.

46 A. Carranza, D. Romero-Perez, H. Almanza-Reyes, N. Bogdanchikova, K. Juarez-Moreno, J. A. Pojman, C. Velasquillo and J. D. Mota-Morales, *Adv. Mater. Interfaces*, 2017, **4**, 1700094.
47 J. L. Robinson, M. A. P. McEnery, H. Pearce, M. E. Whitely, D. J. Muñoz-Pinto, M. S. Hahn, H. Li, N. A. Sears and E. Cosgriff-Hernandez, *Tissue Eng., Part A*, 2016, **22**, 403–414.
48 A. Yu, Y. Zhu, W. Wang and J. Zhai, *Adv. Funct. Mater.*, 2019, **29**, 1900098.
49 A. Kataruka and S. B. Hutchens, *Soft Matter*, 2019, **15**, 9665.
50 A. Kovalenko, K. Zimny, B. Mascaro, T. Brunet and O. Mondain-Monval, *Soft Matter*, 2016, **12**, 5154.
51 A. Rostek, M. Breisch, K. Pappert, K. Loza, M. Heggen, M. Köller, C. Sengstock and M. Epple, *Beilstein J. Nanotechnol.*, 2018, **9**, 2763.
52 Q. Yuan and R. A. Williams, *J. Membr. Sci.*, 2015, **497**, 221.
53 S. Zou, Y. Yang, H. Liu and C. Wang, *Colloids Surf., A*, 2013, **436**, 1.
54 W. D. Bancroft, *J. Phys. Chem.*, 1913, **17**, 501.
55 S. Y. Shin, B. Saravanakumar, A. Ramadoss and S. J. Kim, *Int. J. Energy Res.*, 2016, **40**, 288.
56 M. G. Pérez-García, M. C. Gutierrez, J. D. Mota-Morales, G. Luna-Barcenas and F. del Monte, *ACS Appl. Mater. Interfaces*, 2016, **8**, 16939.
57 H. W. Park, N. D. Huynh, W. Kim, H. J. Hwang, H. Hong, K. Choi, A. Song, K. B. Chung and D. Choi, *Micromachines*, 2018, **9**, 407.
58 J. Young Oh, D. Lee and S. Hyung Hong, *ACS Appl. Mater. Interfaces*, 2018, **10**(25), 2166.